ORIGINAL

Non-Fourier phase change heat transfer in biological tissues during solidification

H. Ahmadikia · A. Moradi

Abstract The phase change in biological tissues during a freezing process is simulated by hyperbolic and parabolic heat equations with temperature-dependent enthalpy. It is observed that the experimental results are in a good agreement with that the calculated results by the enthalpy method. The results shown that the Fourier model predicts tissues temperature lower than of the non-Fourier model. Further decrease in freezing rate and freezing velocity is noticed with an increase in relaxation time value.

1 Introduction

Freezing and thawing phenomena are applied in many industrial and medical applications. Regarding the biological tissues, these phenomena emerge during cryosurgery and cryopreservation processes. The purpose of cryopreservation is to preserve tissues/cells without any significant damage to their function and mechanical properties, viability, etc. [1–4]. The cryopreservation is widely used in stem cell research [5, 6], organs preservation for transplant [7] and engineered tissue products storage and transportation [8]. Biological activities are slow even non-active at the beginning at subzero temperatures. The biological materials' activities are retrieved after the physiological temperature is increased gradually. To guarantee an optimal cooling rate for cryosurgery or cryopreservation, the prediction of the transient temperature distribution of the subject tissues is essential. The cryopreservation cooling rate contributes to the viability of biological tissues cells significantly.

The common phenomena that occur in the tissues solidification process are the extra cellular and intercellular ice formation influenced by the cooling rate. When the cooling rate is low the extra-cellular ice forms and water is transported out of the cell leading to its osmotic dehydration. When cooling rate is high there is not enough time for the water to be transported out of the cell and intracellular ice forms. These phenomena can cause damage to the cells during preserving process. One of the common methods suggested for preserving tissue cells during cryopreservation is rapid freezing. Freezing biological systems at extremely high cooling rates (1,000's of °C/min) lead to solidification. At such a high cooling rate, the ice crystallization and grain growth do not form but a second order thermodynamic phase transition is evolved that leads to an arrest in the translational molecular motions. The frozen region tends to form amorphous ice that is said to have vitrified or formed glass. In order to achieve the cryopreservation of high cooling rate, an increase in the tissue thermal gradient could be considered as an alternative approach. This approach can be adopted by irradiating laser with an ultra short laser pulse that can expose to cryogenic fluid temperatures.

The biological thermal tissues gradient evaluation for the first time was introduced by Fowler and Toner [9]. A new cryopreservation method using laser and liquid nitrogen was adopted by Kandra [10]. In his dissertation, one and two-dimensional computational model of tissue section irradiated by an ultra-short laser pulse and exposed to the cryogenic fluid where adopted where the tissue section

H. Ahmadikia (✉)
Department of Mechanical Engineering, University of Isfahan,
81746-73441 Isfahan, Iran
e-mail: ahmadikia@eng.ui.ac.ir

A. Moradi
Young Researchers Club, Islamic Azad University,
Arak Branch, Arāk, Iran
e-mail: amirmoradi_hs@yahoo.com

cooling rates were evaluated. He applied the parabolic bioheat transfer conduction for modeling a new cryopreservation method. The presence of large ice crystals in food freezing processes, for excellent quality is studied by Sanz et al. [11] for a large section of pork meat frozen by liquid nitrogen evaporation. They applied finite element method for solving governing equations in order to simulate the cooling rates at the product surface. To validate their results, they compared numerical and experimental results and observed a good agreement between them.

In many fields of industrial application the solid–liquid phase change is very extensive including the medical application. Both cryopreservation and cryosurgery are the methods allow for solid–liquid phase change to occur. When this phenomenon occurs in the biological tissues heat transfer, we know that a major difficulty emerges that would be introduced in the non-linearity of the model by the variable disconnection between different phase regions and the unknown position of the solid–liquid interface [12]. Several studies have been conducted on the phase change heat transfer in some industrial applications. Sadd and Didlake [13] were of the first researchers who investigated the phase change in the heat transfer process. They studied melting of a semi-infinite body which was exposed to a sudden temperature difference by the hyperbolic heat conduction problem.

Studholme [14] used the Gibb's free energy for modeling the phase change heat and mass transfer during the freezing process. Sanz and Elvira [15] studied the crystallization process during food freezing. They employed the enthalpy method and the Fourier heat conduction with constant heat properties for freezing modeling. They also used the isothermal phase change for heat transfer modeling on a meat piece and suggested 6 s freezing time for solidification. The effects of non-Fourier heat transfer on prediction of transient temperature and thermal stress in skin cryopreservation are studied by Deng and Liu [16]. At the moving interface for hyperbolic phase change, the temperature is discontinuous, but for simplification, they neglected this in their calculations discontinuity [13, 17]. They found that the non-Fourier effect can be essential when the thermal relaxation time of biomaterials is long. Wang et al. [18] applied the one-dimensional finite difference method in order to simulate the individual food freezing time in the freezing process. They used the apparent heat capacity approach for the phase change modeling. To validate the accuracy of their results, they compared numerical results with the obtained experimental data. An exact analytical solution of three-dimensional phase change heat transport of biological tissue during freezing process was presented by Li et al. [19]. They used the Green function for solving the Fourier heat conduction phase change subject to different boundary conditions.

A review of heat and mass transfer modeling of tissues and cells cryopreservation was perform by Xu et al. [20].

Biological tissues can be treated as porous materials. The desired effects of porous media on freezing and thawing process in tissues were achieved by Kumar and Katiyar [21]. They applied the numerical simulation in order to study the effect of porosity on the motion of freezing and thawing front and transient temperature distribution in the tissue. They observed the significant effects of porosity on the temperature profile and phase change interface. They found that with an increase in the porosity value, the freezing and thawing rates decrease. Other phase change heat transfer studies are reported by Shemetov [22] and Greenberg [23], Alexiades et al. [24], Lu [25], Ayasoufi [26], Wang and Prasad [27], etc.

The objective of this study is to simulate the heat conduction in the tissue cryopreservation. This problem, including the discontinuity of temperature at the solid–liquid interface is solved numerically by the enthalpy method via both parabolic and hyperbolic models. Most researches have neglected the temperature discontinuity for simplicity at the solid–liquid interface [13, 16, 17], but here, two types of phase change (isothermal and non-isothermal) are applied in order to simulate heat transfer in freezing process. In most solidification systems, however, the phase change from liquid to solid and the accompanying evolution of latent heat will occur over a temperature range where both the solid and liquid coexist [28]. In this study, the linear evolution of latent heat over the solidification range is used for the non-isothermal phase change. The influence of this discontinuity and the relaxation time on the temperature distribution through the subject tissues, cooling rate and freezing position are studied and different results are obtained for the parabolic and hyperbolic models.

2 Mathematical formulations

2.1 The hyperbolic heat transfer formulation for the enthalpy method during freezing process

The numerical solution of the hyperbolic phase change heat transfer in skin cryopreservation was solved numerically by the implicit method by Deng and Liu [16]. They ignored the temperature discontinuity at the phase change. Here, for numerical solution, the temperature at the moving interface is considered discontinuous. The enthalpy method in the fixed grid is applied for the numerical solution of the parabolic and hyperbolic heat transfer during freezing process.

The one-dimensional hyperbolic heat transfer equation using the enthalpy method can be presented as:

$$\frac{\partial e}{\partial t} + \tau \frac{\partial^2 e}{\partial t^2} = \frac{\partial}{\partial x}\left(k\frac{\partial T}{\partial x}\right) + g \tag{1}$$

where, g is the sink or source of the heat, τ is the relaxation time, k is the thermal conductivity and e is the enthalpy per unit volume. In two phases control volume, the combinational thermal conductivity coefficient is calculated by:

$$\frac{1}{k_{sl}} = \frac{f}{k_l} + \frac{1-f}{k_s} \tag{2}$$

where, k_{sl} is the combinational thermal conductivity of two phases control volume with the volume fraction f, and the enthalpy of two phases control volume is expressed by:

$$e = (1-f)e_s + fe_l \tag{3}$$

where, e_s and e_l are the enthalpy of solid and liquid phases respectively in the control volume. The combinational specific heat and density of two phases control volume are defined by:

$$C_{sl} = (1-f)C_s + fC_l \tag{4}$$

$$\rho_{sl} = (1-f)\rho_s + f\rho_l \tag{5}$$

where, C_{sl} and ρ_{sl} are the combinational specific heat and density in two phases control volume, respectively. In general, the enthalpy can depend on different parameters like temperature, cooling rate, heating rate, etc. In most studies, the temperature-dependent enthalpy is considered for two phases modeling. In this article, the same concept is followed for the solid–liquid modeling in cryopreservation.

2.2 Isothermal phase change

For a material that changes phase at temperature $T < T_s$, the function of the enthalpy-temperature is defined by:

$$e_s = \int_{T_{ref}}^{T} \rho_s C_s dT \quad T < T_s \tag{6}$$

where, T_s and T_{ref} are the freezing and base temperature, respectively. In this case, because the whole control volume is in the solid phase, the latent heat is not considered; hence, the volume fraction of the unfrozen phase is zero. When the phase change begins, the temperature is T_s; thus, the enthalpy-temperature function is expressed by:

$$e_{sl} = e_s|_{T=T_s} + H_L \quad T = T_s \tag{7}$$

where, e_{sl} is the enthalpy of material during phase change and H_L is the latent heat of phase change defined by:

$$H_L = fL \tag{8}$$

where, L is the latent heat of the whole phase change process. When the material temperature is greater than freezing temperature $(T > T_s)$, the enthalpy-temperature function is expressed by:

$$e_l = e_{sl}|_{T=T_l} + \int_{T_s}^{T} \rho_l C_l dT \quad T > T_s \tag{9}$$

where, T_l is the thawing temperature and the volume fraction is one.

2.3 Non-isothermal phase change

For a non-isothermal phase change, the fusion occurs over the temperature range $T_s < T < T_l$, and the volume fraction f changes from a step function into other forms that may or may not contain a discontinuity phase. For this type of problem, when $T < T_s$, the enthalpy function is calculated by Eq. (6). In the unfrozen zone, however, the liquid fraction needs to be defined at each point. The liquid fraction can be a function of a number of solidification variables [19]. In many systems, it is reasonable to assume that the liquid fraction is just a temperature function. The linear temperature-dependent enthalpy is considered for the non-isothermal phase change. When the material temperature is $T_s \leq T \leq T_l$, the enthalpy function is defined by:

$$e_{sl} = e_s|_{T=T_s} + \int_{T_s}^{T} \rho_{sl} C_{sl} dT + H_L \quad T_s \leq T \leq T_l \tag{10}$$

The above variables were defined in the previous section. For $T > T_l$, the enthalpy is defined by:

$$e_l = e_{sl}|_{T=T_l} + \int_{T_l}^{T} \rho_l C_l dT \quad T > T_l \tag{11}$$

3 The numerical solution for the enthalpy method

Numerical application of these methods gives better results when the phase change occurs within a specific temperature range. The temperature distribution and volume fraction of solid and liquid phases are obtained by enthalpy in this newly presented method. Easy development of enthalpy method compared to the multi-dimensional and other heat transfer models such as: thermal wave and DPL (dual-phase-lag) models are the advantages of this method [28, 29].

The finite difference scheme is applied to discretize the governing equations and boundary conditions. The explicit form of finite difference for Eq. (1) by allowing for $g = 0$ can be presented as:

$$(\Delta t + \tau)e_i^{n+1} - (\Delta t + 2\tau)e_i^n + \tau e_i^{n-1}$$
$$= \frac{\Delta t^2}{\Delta x^2} \left[k_{aven} \left(T_{i-1}^n - T_i^n \right) + k_{aves} \left(T_{i+1}^n - T_i^n \right) \right] \quad (12)$$

where, Δt and Δx are the time and space steps, respectively, k_{aven} is the average thermal conductivity at nodes i and $i-1$ and k_{aves} is the average thermal conductivity at nodes i and $i+1$.

The Von Neumann analysis [30] is employed here for stability analysis and can provide a necessary stability criterion for a numerical scheme expressed as:

$$\frac{\alpha \Delta t (2\Delta t + 4\tau_T)}{\Delta x^2 (\Delta t + 2\tau_q)} \leq 1, \quad \alpha = \max(\alpha_s, \alpha_l) \quad (13)$$

where, α_s and α_l are thermal diffusivity of solid and liquid phases, respectively. The stability criterion of Eq. (13) is derived for one phase without heat sources. The enthalpy of each grid is calculated by:

$$e_i^{n+1} = c_2 e_i^n + c_3 e_i^{n-1}$$
$$+ c_4 \left[k_{aven} \left(T_{i-1}^n - T_i^n \right) + k_{aves} \left(T_{i+1}^n - T_i^n \right) \right] \quad (14)$$

where, $c_1 = dt + \tau$, $c_2 = (\Delta t + 2\tau)$, $c_3 = -\tau/c_1$ and $c_4 = (\Delta t/\Delta x)^2 / c_1$.

In this study, an independent-temperature thermal conductivity is considered. While the different values of thermal conductivity are considered for frozen and unfrozen zones, the thermal conductivity during phase change is obtained by:

$$k_{aven} = \frac{2k_l k_s}{k_s f_i^n + k_l(1 - f_i^n) + k_s f_{i-1}^n + k_l(1 - f_{i-1}^n)} \quad (15)$$

$$k_{aves} = \frac{2k_l k_s}{k_s f_i^n + k_l(1 - f_i^n) + k_s f_{i+1}^n + k_l(1 - f_{i+1}^n)} \quad (16)$$

where, f is the volume fraction of unfrozen phase. In this case, the average thermal conductivity of new time step during phase change is calculated using the volume fraction of unfrozen phase of the previous time step. In this research, the density change and material deformation are ignored during solidification and phase change. The specific heat value is considered constant and different at each phase.

For a material that changes phase at a single temperature T_s (isothermal phase change), the enthalpy of the liquid and solid can be calculated by:

$$e_s = \rho C_s T_s \quad (17)$$

$$e_l = \rho C_s T_s + \rho L \quad (18)$$

These values can also be used in the numerical approach for determining whether each grid element is solid, liquid or is undergoing the thawing/freezing process. For this type of problem, the temperature field can be calculated by:

$$T = \begin{cases} T = e/\rho C_s & (e < e_s) \\ T = T_s & (e_s \leq e \leq e_l) \\ T = \left(\frac{e}{\rho} + T_s(C_l - C_s) - L \right) / C_l & (e > e_l) \end{cases}$$
$$(19)$$

For the two phase zone, the volume fraction of liquid is obtained by:

$$f = (e - e_s)/(e_l - e_s) \quad e_s \leq e \leq e_l \quad (20)$$

All these parameters are calculated in each time step. For the non-isothermal phase change (linear temperature-dependent enthalpy), the enthalpies per unit volume of the fusion solid and the fusion liquid are defined in the following equations, respectively.

$$e_s = \rho C_s T_s \quad (21)$$

$$e_l = \rho C_s T_s + \rho C_{ave}(T_l - T_s) + \rho L \quad (22)$$

where, C_{ave} is the average specific heat. For this type of problem, the temperature field can be calculated by:

$$T = \begin{cases} T = e/\rho C_s & (e < e_s) \\ T = T_s + (T_l - T_s)\left(\frac{e - e_s}{e_l - e_s}\right) & (e_s \leq e \leq e_l) \\ T = \left(\frac{e}{\rho} + C_s T_s - C_{ave}(T_l - T_s) + C_l T_l - L \right) / C_l & (e > e_l) \end{cases}$$
$$(23)$$

Here, the two important parameters are the freezing velocity and the freezing rate. The freezing velocity is the distance that the final point of solidification process moves per unit of time; the freezing rate for each point of the tissue is defined by the amount of temperature drop during complete solidification process per unit of time and defined as:

$$\text{freezing velocity} = \frac{\Delta x}{t_{fn_i} - t_{fn_{i-1}}} \quad (24)$$

$$\text{freezing rate}_i = \left(T_{ini_i} - T_{final} \right) / t_{fn_i} \quad (25)$$

where, T_{ini_i} and T_{final} are the initial temperatures of point i before cooling process begins and final temperature of point i after cooling process ends, respectively; $t_{fn_{i-1}}$ is the time of complete solidification at point $(i - 1)$ and t_{fn_i} is the final time of solidification process at point i.

4 Results and discussion

4.1 Case study and validation of numerical simulation

In this article, the numerical results are shown for the parabolic and hyperbolic heat transfer with phase change during the solidification process. The grid-dependence test is first conducted by using several different size meshes.

For the grid study, a slice of beef with $x = 0.02$ m length is selected; the beef properties have been reported by Wang et al. [18]. The time step and relaxation time (in the hyperbolic model) for the numerical solution are $\Delta t = 10^{-6}$ and $\tau = 0.1$ s, respectively. The beef slice is frozen symmetrically on both sides with constant temperature 77 K and the initial temperature is $T_0 = 300$ K. The effect of mesh size and time step on the hyperbolic beef temperature are studied.

The numerical results with the experimental data obtained by Tu and Liu [31] for a slice of cucumber are compared in Fig. 1. Wang et al. [18] applied this experimental data for validate of their simulation results. The cucumber thickness is 2.5 cm and the insulated boundary condition at the center of cucumber ($x = 1.25$ cm) and convection condition with air $-40\,^{\circ}$C and $h = 280$ W/m^2 $^{\circ}$C are considered as the boundary conditions. The initial temperature of cucumber is $T = 293$ K and the cucumber properties were described in the refs. [18, 31]. The temperature at the center of the cucumber slice (temperature at $x = 1.25$ cm) of test object versus time for numerical and experimental analysis is shown in Fig. 1. It is worth mentioning that the obtained temperature distribution in validating the study is calculated from the parabolic heat transfer model with phase change during solidification process. As illustrated in Fig. 1, there exists an excellent agreement between the numerical results and the experimental data. It can be deduced that the enthalpy method is a good method for predicting thermal behaviors of biological materials during phase change in solidification process.

4.2 The numerical results for the hyperbolic non-isothermal phase change

In order to investigate the non-isothermal phase change during the solidification process, a beef tissue of length $x = 0.01$ m with the initial temperature $T_0 = 300$ K is selected. At $t = 0$, the surface temperature at $x = 0$ drops to the fusion temperature of liquid nitrogen 77 K and is maintained at that value. The surface at $x = 0.01$ m is insulated. The beef tissue properties were presented in Ref. [18] and the relaxation time is $\tau = 0.3$ s. The temperature profiles of hyperbolic model for three different points of the beef tissue ($x = 0.0025$, 0.005, 0.01 m) are illustrated in Fig. 2. As expected, the tissue temperature for closer points to $x = 0$ is lower than that of the farther points. In general, the solidification process for closer points to the cooling boundary occurs at the shorter time than the farther points. As shown in Fig. 2, when the temperature of each point in the tissue reaches to $T_m = 272.65$ K (thawing temperature), a portion of the cooling energy is wasted by the latent heat, afterwards this temperature reaches to $T_s = 269.15$ K (freezing temperature). With the passage of time, the slope of temperature profile becomes lower and the interface velocity of phase change decreases as well. After solidification process, when whole of tissue is frozen, the thermal conductivity and the thermal diffusivity of the frozen phase become greater than the unfrozen phase. Thus, the temperature profile slope and freezing velocity increase again. Because of the low difference temperature between the tissue and the cooling boundary, the slope of temperature profile and freezing velocity decrease again.
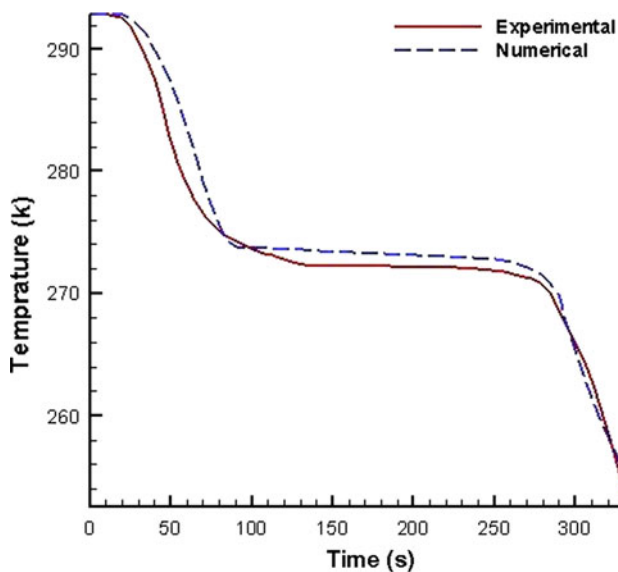

Fig. 1 The comparison between the present numerical results obtained from the parabolic model and experimental data [31] for the central temperature of a slice of cucumber
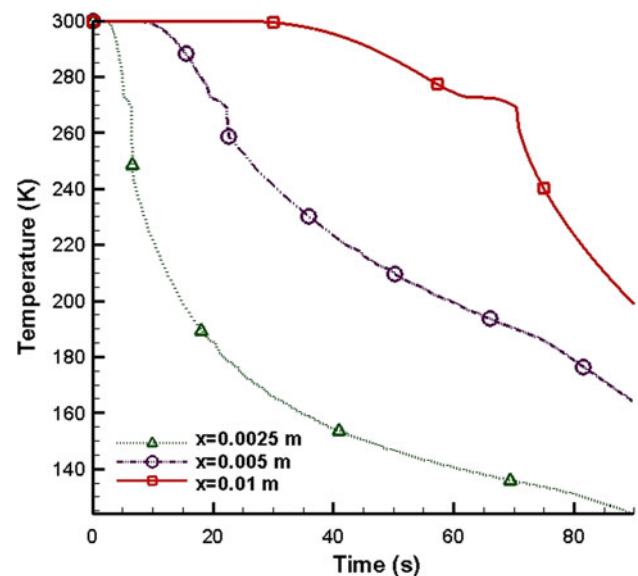

Fig. 2 The variations of temperature versus time for three different points of beef tissue in non-isothermal phase change via the hyperbolic model ($\tau = 0.3$ s)
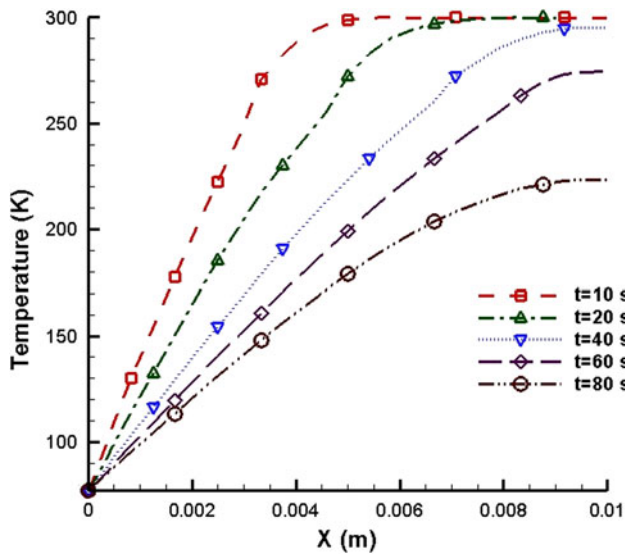
Fig. 3 The variation of temperature along the beef tissue for different times in non-isothermal phase change via the hyperbolic model ($\tau = 0.3$ s)

Fig. 5 The freezing velocity versus time for a beef tissue and the hyperbolic model ($\tau = 0.3$ s)

Figure 3 shows the temperature distribution in the subject beef tissue at time intervals $t = 10$, 20, 40, 60, and 80 s for hyperbolic case with $\tau = 0.3$ s. As the time increases, the temperature distributions in the beef tissue converge together. At the beginning of the solidification process, the end parts of the beef tissue would not freeze; but as time goes on, whole beef tissue freezes, because of the higher thermal conductivity and diffusivity in the frozen zone rather than the unfrozen zone, the freezing velocity increases.

The position of the phase change interface versus time for the beef tissue is shown in Fig. 4. With an increase in

time, the slope of freezing position decreases, and due to being away from the cooling boundary, the temperature gradient decreases as well. The interface velocity versus time for the beef tissue is shown in Fig. 5. As can be observed, at the beginning, the freezing velocity is high; while interface velocity decreases with an increase in time. As mentioned, with the tissue depth solidification, the temperature gradient becomes smaller. Hence, the freezing velocity and freezing rate decrease. The freezing rate up to the end of solidification process along the beef tissue is illustrated in Fig. 6. The intracellular and extra cellular ice formations are common phenomena, affected by freezing

Fig. 4 The variation of freezing position versus time for a beef tissue and the hyperbolic model ($\tau = 0.3$ s)

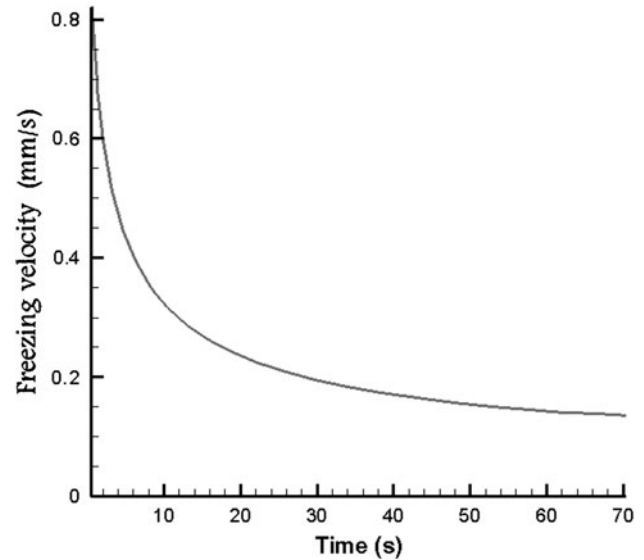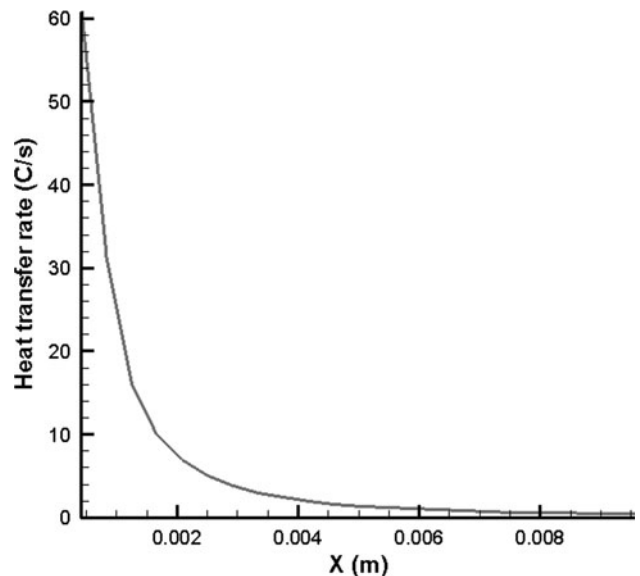**Fig. 6** The variation of freezing rate along the beef tissue for the non-isothermal phase change and the hyperbolic model ($\tau = 0.3$ s)

rate. As expected, in the closer zones to the cooling boundary the cooling rate is higher than that of the farther zones. For the farther zones the cooling rate decreases drastically. This phenomenon leads to the large ice crystals formation that may damage the cells during preserving process.

4.3 The effect of thermal relaxation on the solidification process

A beef tissue of length $x = 0.01$ m same as the one in Sect. 4.2 is selected here. A comparison of the hyperbolic results with the small relaxation time ($\tau = 0.1$) to the corresponding parabolic solution is a logical way to validate the numerical scheme for the hyperbolic phase change problems. The temperature profiles along the beef tissue at $t = 90$ s are shown in Fig. 7 for parabolic ($\tau = 0$) and hyperbolic ($\tau = 0.1$ and $\tau = 0.3$) solutions. It is well known that when τ approaches zero, the hyperbolic solution approaches the parabolic solution. In Fig. 7, the temperature profile for $\tau = 0.1$ and $\tau = 0$ is almost identical; while, as τ increases the discrepancy between the hyperbolic and parabolic solutions becomes evident.

For both parabolic and hyperbolic ($\tau = 0.25$ s and $\tau = 0.45$ s) models the temperature distribution for the end of the beef tissue ($x = 0.01$ m) versus time is shown in Fig. 8. As illustrated here, the tissue temperature for the hyperbolic model at the same time is higher than the parabolic model. With an increase in the thermal relaxation time, the temperature increases in the tissue. For example, tissue temperature for $\tau = 0.45$ s is higher than $\tau = 0.25$ s.
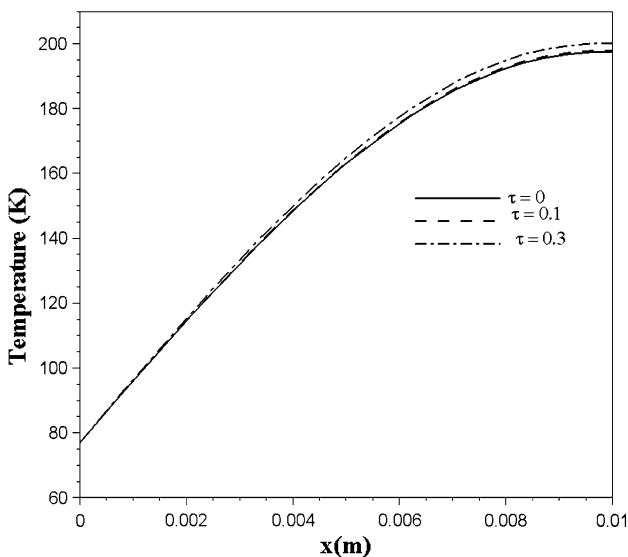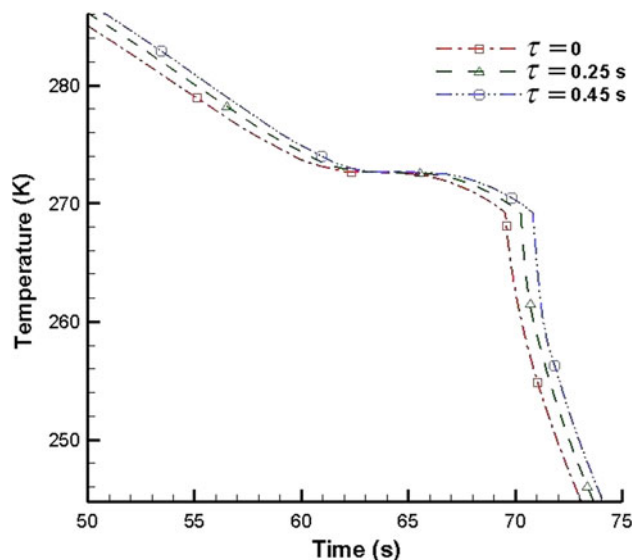

Fig. 8 Comparison of the beef temperature for both hyperbolic ($\tau = 0.25$, 0.45 s) and parabolic non-isothermal phase change model for $x = 0.01$ m

This can be qualitatively analyzed as follow: the energy for the low τ case diffuses into the beef tissue much quicker; hence, the tissue solidifies faster and the tissue temperature decreases more compared to high τ case. The temperature distribution in a point of the tissue ($x = 0.0025$ m) for both parabolic and hyperbolic models is illustrated in Fig. 9. Similar to the results deduced from Fig. 8, the parabolic model predicts lower temperature for tissues than the hyperbolic model at the same time. By comparing Figs. 8 and 9, it is deduced that the discrepancy between the
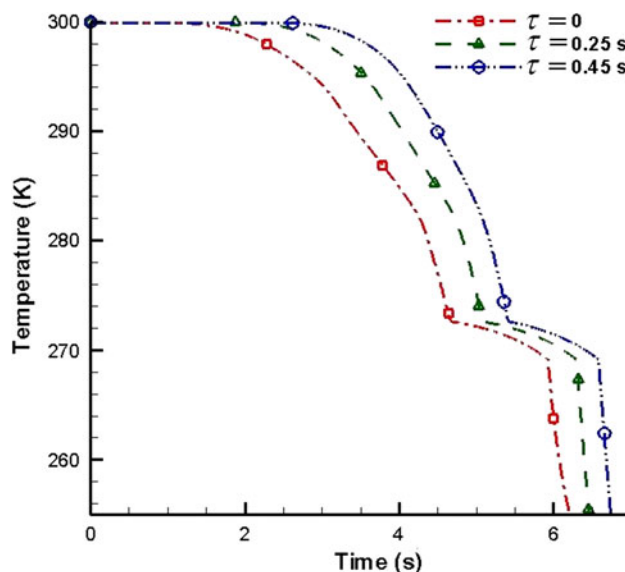

Fig. 7 Comparison of the beef temperature for both hyperbolic ($\tau = 0.1$, 0.3 s) and parabolic non-isothermal phase change model at $t = 90$ s

Fig. 9 Comparison of the beef temperature for the hyperbolic ($\tau = 0.25$, 0.45 s) and parabolic non-isothermal phase change model for $x = 0.0025$ m

hyperbolic and parabolic models for closer points to the cooling boundary ($x = 0.0025$ m) is higher than that of the farther points ($x = 0.01$ m). Because the temperature gradient at the closer points to the cooling boundary is severe, subsequently the effect of thermal relaxation time on the temperature distribution is more evident.

Figure 10 illustrates how freezing position is affected by changes in the thermal relaxation time. According to Fig. 10, the freezing position for the parabolic model moves faster than the hyperbolic one. This means that the phase change interface position for the parabolic case at the same time is greater than that of the hyperbolic case. Furthermore, with an increase in the thermal relaxation time, the phase change interface moves slower.

The freezing velocity of the beef tissue for both parabolic and hyperbolic models is illustrated in Fig. 11. As expected, the freezing velocity for the parabolic model is higher than that of the hyperbolic model and as the freezing velocity decreases, the thermal relaxation time increases. As shown in Fig. 11, the discrepancy between the parabolic and hyperbolic models at the beginning is clear. This is the result of severe temperature gradient at beginning.

The effect of the thermal relaxation time on the cooling rate for the part of beet tissue up to the complete solidification process is shown in Fig. 12. As expected, the parabolic model predicts the higher freezing rate than the hyperbolic model. This indicates that as the relaxation time increases, the non-Fourier effect becomes more prominent. Just like Fig. 11, here in the closer points to the cooling boundary, the difference solution between both parabolic and hyperbolic models is more evident.
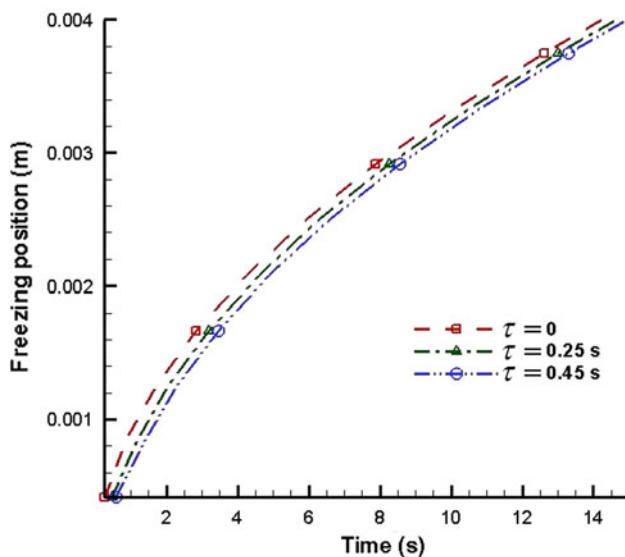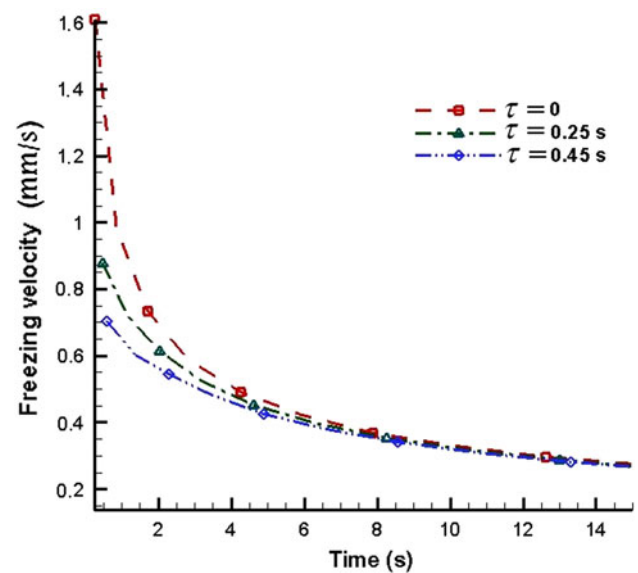

Fig. 11 The freezing velocity versus time for both hyperbolic ($\tau = 0.25$, 0.45 s) and parabolic non-isothermal phase change model of a beef tissue
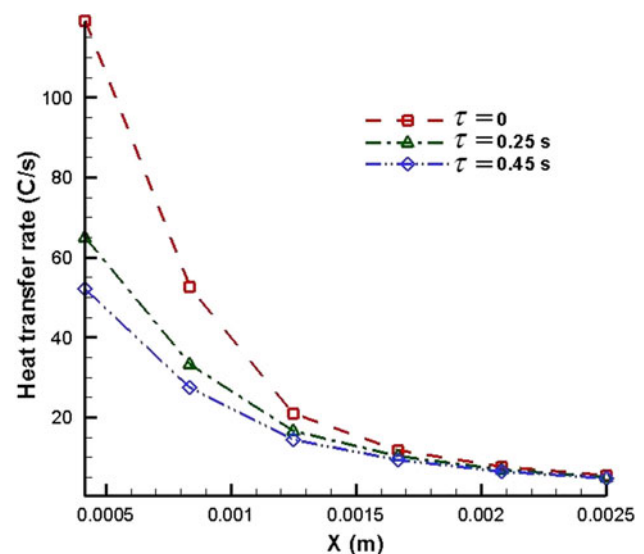

Fig. 12 Comparison of freezing rate for both hyperbolic ($\tau = 0.25$, 0.45 s) and parabolic non-isothermal phase change model of a beef tissue

4.4 The numerical results for the hyperbolic isothermal phase change

In order to investigate the isothermal phase change during cryopreservation, the skin tissue with $x = 0.01$ m length is selected here. The skin properties are same as the recorded in Ref. [16]. The boundary and initial conditions are same as what is in Sect. 4.2. Here thermal relaxation time for the
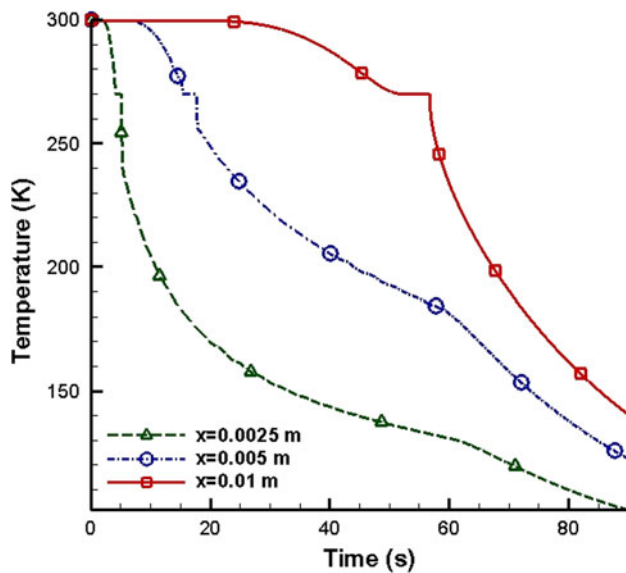

Fig. 10 Comparison of freezing position for both hyperbolic ($\tau = 0.25$, 0.45 s) and parabolic non-isothermal phase change of a beef tissue

Fig. 13 The variations of temperature versus time for three different points of skin tissue in isothermal phase change by the hyperbolic ($\tau = 0.2$ s) model

Fig. 14 Comparison of the skin temperature for both hyperbolic ($\tau = 0.1$, 0.3 s) and parabolic isothermal phase change for $x = 0.001$ m

skin tissue is $\tau = 0.2$ s. The temperature distribution of three points in skin tissue for the hyperbolic model is shown in Fig. 13. It is clear that for the closer zones to the cooling boundary the skin temperature decreases drastically, while in the zone farther from the cooling boundary the slope of temperature profile becomes smaller gradually. In this case, when the freezing process reaches each one of the zones in the tissue, the phase change occurs at the constant temperature and the latent heat of the tissue is achieved at this temperature (freezing temperature T_s). As shown in Fig. 13, for closer zones to the cooling boundary, the phase change process occurs in a shorter time. Figure 14 illustrates that how the temperature profile of end skin tissue ($x = 0.01$ m) is affected by the relaxation time. As mentioned in the previous section, the parabolic model predicts the temperature lower than the hyperbolic model at the same time. This means that for the parabolic model, the solidification process ends earlier than the hyperbolic model. The skin temperature increases, when the thermal relaxation time increases. The variation of temperature at $x = 0.0025$ m in the isothermal phase change process for both parabolic and hyperbolic models is illustrated in Fig. 15. Similar to Fig. 14, at the same time, the hyperbolic temperature is higher than the parabolic model. Here, for closer zones to the cooling boundary, the discrepancy between the Fourier and non-Fourier models is more evident than the farther zones. Both the isothermal and non-isothermal types of phase change are observed in Figs. 15 and 8, respectively. In Fig. 8, the phase change occurs in a limited interval of temperature, while in Fig. 15, the phase change process occurs in the constant temperature.
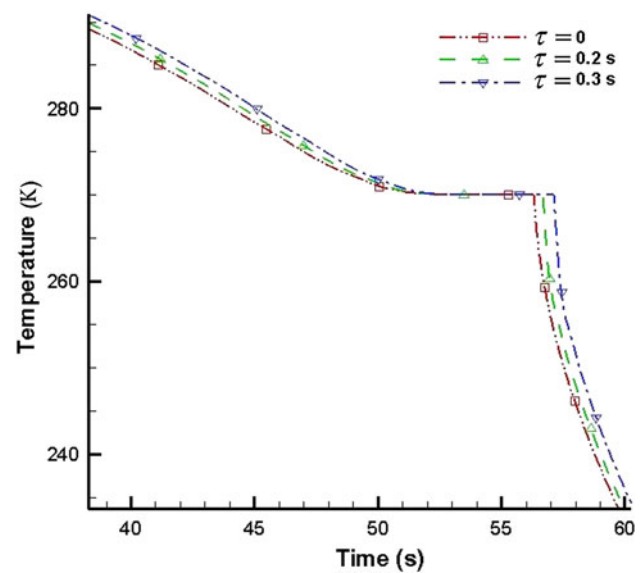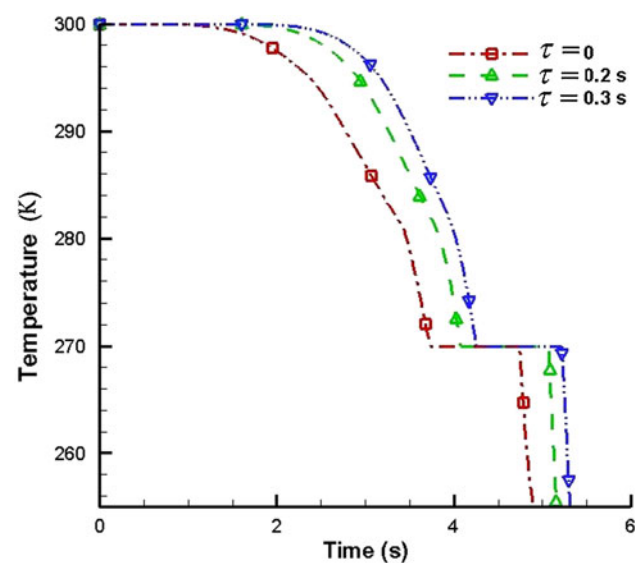

Fig. 15 Comparison of the skin temperature for both hyperbolic ($\tau = 0.1$, 0.3 s) and parabolic isothermal phase change for $x = 0.0025$ m

5 Conclusions

In this article, the phase change process inside different tissues subject to freezing process is studied numerically with respect to the non-Fourier effect. For the numerical solution, the enthalpy method is applied with respect to the isothermal and non-isothermal phase changes. To validate the numerical scheme, the parabolic numerical results are compared with the experimental data that were presented

by Tu and Liu [31] on a slice of cucumber. The comparison between the hyperbolic results with the small relaxation time with the parabolic results was used to validate the numerical solution for the hyperbolic phase change during cryopreservation. For the shorter thermal relaxation time, it was observed that the hyperbolic solution was able to approach the parabolic solution. Comparing the long relaxation time parameter with the short relaxation time parameter, it was observed that as relaxation time increases, the non-Fourier effect becomes more effective. The freezing velocity and freezing rate were decreased when the relaxation time was increased. The discrepancy between the isothermal and non-isothermal phase change results is evident. The results indicate that the enthalpy method has a high capability to solve heat conduction problems in the solidification process.

References

1. Whittingham DG, Leibo SP, Mazur P (1972) Survival of mouse embryos frozen to −196 °C and −269 °C. Science 178:411–414
2. Ludwig M, Al-Hasani S, Felderbaum R, Diedrich K (1999) New aspects of cryopreservation of oocytes and embryos in assisted reproduction and future perspectives. Hum Reprod 14:162–185
3. Agca Y (2000) Cryopreservation of oocyte and ovarian tissue. ILAR J 41:207–220
4. Stachecki JJ, Cohen J (2004) An overview of oocyte cryopreservation. Reprod Biomed Online 9:152–163
5. Bakken AM (2006) Cryopreserving human peripheral blood progenitor cells. Curr Stem Cell Res Ther 1:47–54
6. Hunt CJ, Timmons PM (2007) Cryopreservation of human embryonic stem cell lines. Methods Mol Biol 368:261–270
7. Ishine NB, Rubinsky C, Lee Y (2000) Transplantation of mammalian livers following freezing: vascular damage and functional recovery. Cryobiology 40:84–89
8. Nerem RM (2000) Tissue engineering: confronting the transplantation crisis. Proc Inst Mech Eng 214:95–99
9. Fowler AJ, Toner M (1997) Cryopreservation of cells using ultrarapid freezing. J Heat Transf 37:179–183
10. Kandra D (2001) Tissue interactions with lasers and liquid nitrogen—a novel cryopreservation method. MSc thesis, Department of mechanical engineering, Bangalore University
11. Sanz PD, de Elvira C, Martino M, Zaritzky N, Otero L, Carrasco JA (1999) Freezing rate simulation as an aid to reducing crystallization damage in foods. Meater Sci 52:275–278
12. Deng ZS, Liu J (2004) Modeling of multidimensional freezing problem during cryosurgery by the dual reciprocity boundary element method. Eng Anal Bound Elem 28(2):97–108
13. Sadd MH, Didlake JE (1977) Non-Fourier melting of a semi-infinite solid. ASME J Heat Transf 99:25–28
14. Studholme CV (1977) Modeling heat and mass transport in biological tissue during freezing. MSc thesis, Department of Mathematical Science, Edmonton, Alberta
15. Sanz PD, de Elvira C (1998) Freezing rate simulation as an aid to reducing crystallization damage in foods. Meater Sci 52:275–278
16. Deng ZS, Liu J (2003) Non-Fourier heat conduction effect on prediction of temperature transients and thermal stress in skin cryopreservation. J Therm Stress 26:779–798
17. DeSocio LM, Gualtieri G (1983) A hyperbolic Stefan problem. Q Appl Math 41:253–259
18. Wang Z, Wu H, Zhao G (2006) One-dimensional finite-difference modeling on temperature history and freezing time of individual food. J Food Eng 79:502–510
19. Li FF, Liu J, Yue K (2009) Exact analytical solution to three dimensional phase change heat transfer problems in biological tissues subject to freezing. Appl Math Mech 30(1):63–72
20. Xu F, Moon S, Zhang X, Shao L, Song YS, Demirci U (2010) Multi-scale heat and mass transfer modeling cell and tissues cryopreservation. Phil Trans R Soc A 368:561–583
21. Kumar S, Katiyar VK (2010) Mathematical modeling of freezing and thawing process in tissues: a porous media approach. Int J Appl Mech 2(3):617–633
22. Shemetov NV (1991) The Stefan problem for a hyperbolic heat equation. Int Ser Numer Math 99:365–376
23. Greenberg JM (1987) A hyperbolic heat transfer problem with phase changes. IMA J Appl Math 38:1–21
24. Alexiades ADV, Wilson DG, Drake J (1985) On the formulation of hyperbolic Stefan problems. Q Appl Math 43:295–304
25. Lu WQ (1998) The energy balance condition on the interface for phase change with thermal wave. Int J Heat Mass Transf 41:1357–1359
26. Ayasoufi A (2004) Numerical simulation of heat conduction with melting and/or freezing by space-time conservation element and solution element method. Ph. D Dissertation, Collage of Engineering, University of Toledo
27. Wang GX, Prasad V (2000) Microscale heat and mass transfer and non-equilibrium phase change in rapid solidification. Mater Sci Eng A 292:142–148
28. Swaminathan CR, Voller VR (1992) A general enthalpy method for modeling solidification processes. Metall Trans B 23B:651–664
29. Voller VR, Swaminathan CR (1991) General source-based method for solidification phase change. Numer Heat Transf Part B 19:175–189
30. Tannehill JC, Anderson DA, Pletcher RH (1997) Computational fluid mechanics and heat transfer, 2nd edn. Taylor & Francis, Washington, DC
31. Tu JX, Liu BL (2000) Numerical simulation and experimental study on the freezing process of cucumber. J Univ Shanghai Sci Technol 22(4):304–307